https://doi.org/10.5194/tc-2022-106
Preprint. Discussion started: 20 June 2022

The Cryosphere Discussions

Validation of a fully-coupled radiative transfer model for sea ice with albedo and transmittance measurements

Zhonghai Jin[1], Matteo Ottaviani[1,2], Monika Sikand[3]

[1]NASA Goddard Institute for Space Studies, New York, NY, USA

[2]Terra Research Inc, Hoboken, NJ (USA)

[3]Department of Applied Physics and Applied Mathematics, Columbia University, New York, NY (USA)

Correspondence to: Zhonghai Jin (zhonghai.jin@nasa.gov)

Abstract. A rigorous treatment of the sea ice medium has been incorporated in the advanced Coupled Ocean-Atmosphere Radiative Transfer (COART) model. The inherent optical properties (IOPs) of brine pockets and air bubbles over the 0.25-4.0 μm spectral region are parameterized as a function of the vertical profile of the sea ice physical properties (temperature, salinity and density). We test the model performance using available albedo and transmittance measurements collected during the Impacts of Climate on the Ecosystems and Chemistry of the Arctic Pacific Environment (ICESCAPE) and the Surface Heat Budget of the Arctic Ocean (SHEBA) field campaigns. The observations are adequately simulated when at least three layers are used to represent bare (first-year and multi-year) ice, including a thin top layer characterized by low density and high scattering. Two layers can be sufficient to model isolated cases of multi-year ice, and apply well to ponded ice except for shallow ponds over thick ice. The albedo and transmittance of ponded ice in the visible are mainly determined by the optical properties of the ice underlying the water layer used to model the pond. Sensitivity results indicate that the air volume or ice density has the largest impact on the simulated fluxes. Possible contamination from light-absorbing impurities, such as black carbon or ice algae, is also implemented in the model and is able to effectively reduce the albedo and transmittance in the visible spectrum to further improve the model-observation agreement. The agreement between the observed and modeled spectra validates the parameterization of the sea ice IOPs, and endorses COART as an accurate tool for radiation studies in the cryosphere.

1 Introduction

Sea ice is a vital component of the global climate system, since it affects heat and moisture exchange within the atmosphere and ocean, and strongly impacts the surface energy budget (Fetterer et al., 2002; Serreze and Barry, 2011; Kwok and Untersteiner, 2011; Stroeve et al., 2012). A reduction in sea ice cover lowers the albedo and increases shortwave absorption in the ocean, causing more melting in a mechanism known as ice-albedo feedback (Curry et al., 1995; Hall, 2004; Déry and Brown, 2007), which has been quantified as the second main contributor to the Arctic amplification using climate simulations (Taylor et al., 2012; Pithan and Mauritsen, 2014). The interactions between snow, sea ice and solar radiation in most climate models are based on empirical parameterizations that are often just a function of snow depth, sea ice thickness and surface temperature. However, an accurate description of the interaction between sea ice and solar radiation also requires adequate estimations of the multiple scattering processes and the absorption rate within the ice column. To improve our confidence in model projections of sea ice extent and thickness, it is therefore crucial to develop accurate and efficient radiative transfer models. A detailed characterization of the optical behavior of sea ice is even more important since the latter changes dramatically in response to structural variations, as a freezing water surface grows into a stable pack, to then age and undergo possible melting (Grenfell and Maykut, 1977; Weeks and Ackley, 1986, Hunke et al., 2011; Warren 2019). The first stages of sea-ice formation are associated with the phase transition, and are characterized by increasing salinity, viscosity and elasticity (Daly, 1994; Dmitrenko et al., 2010). “Young ice” of a thickness up to 30 cm, that can still be fractured by wave motion,

https://doi.org/10.5194/tc-2022-106
Preprint. Discussion started: 20 June 2022

evolves eventually into more stable first-year ice (FYI) of thickness of up to 2m (Notz et al., 2008). If FYI survives the first melting season, it ages into multi-year ice (MYI) which typically exhibits thicknesses up to 3m or more, and a decrease in density and salinity mainly caused by an increase of air volume and the flushing of brine (Eicken et al., 1995; Nicolaus et al., 2012). If a bare MYI surface is exposed, it commonly exhibits a blue tint because bubbles act as scattering centers. The reported values of sea ice density vary over a wide range, from 0.72 g/cm^3 to 0.94 g/cm^3 (Timco and Frederking, 1995).

Field and remote sensing observations of the spectral albedo, spectral transmittance, and extinction coefficients have been reported for a variety of the ice types mentioned above (Light et., 2008, hereafter referred to as L08; Light et al., 2015, hereafter referred to as L15; Grenfell and Perovich, 1984; Perovich et al. 2002; Ehn et al., 2006; Untersteiner, et al., 2007; Nicolaus et al. 2007; Taskjelle et al., 2015). However, simultaneous observations of entire vertical columns in the cryosphere, including vertical profiles of the sea ice physical properties, have traditionally been sparse. Notable field campaigns include The First International Satellite Cloud Climatology Project (ISCCP) Regional Experiment (FIRE) Arctic Clouds Experiment (FIRE ACE, Curry et al. 2000), the Surface Heat Budget of the Arctic Ocean (SHEBA, Perovich et al. 2002), and the Impacts of Climate on the Ecosystems and Chemistry of the Arctic Pacific Environment (ICESCAPE, L15). Fortunately, large campaigns such as the recently concluded Multidisciplinary drifting Observatory for the Study of Arctic Climate (MoSAIC, Nicolaus et al., 2022) and the planned Arctic Radiation-Cloud-Aerosol-Surface Interaction Experiment (ARCSIX, Schmidt et al., 2021) will provide large datasets to complement the observations from SHEBA and ICESCAPE with increased instrumentation and technological capabilities.

Radiation measurements as those collected in the campaigns listed above are critical for the validation of radiative transfer models. Efforts to simulate sea-ice albedo and transmittance measurements are reported in a few dedicated studies. Grenfell (1991) employed a four-stream, discrete-ordinate radiative transfer code to investigate light propagation within sea ice, a model thereafter used by L08 and L15. Briegleb and Light (2007) employed the Delta-Eddington scheme in a climate model. Jin et al. (1994) developed a broadband multiple-stream, coupled radiative transfer model to investigate the solar radiation distribution and absorption in the polar atmosphere, sea ice and ocean system. This model was also used by Hamre et al. (2004) to study short-wave transmission through first-year thin ice. Taskjelle et al. (2015) applied the derivative AccuRT software (Hamre et al., 2017) to retrieve the properties of newly formed (very thin) ice. As described in the next section, Jin et al. (2006) developed a Coupled Ocean-Atmospheric Radiative Transfer (COART) model, which has flexible and high spectral resolution up to 0.1 cm^{-1} to accurately account for the atmospheric absorptions and has included the surface roughness parameter in the radiative transfer solution. Here, we extend the previously validated (Jin et al., 2002; 2005) COART model to include the sea ice medium, in order to rigorously calculate the radiative distribution in the atmosphere-sea ice-ocean system. The sea ice optical properties are directly parameterized as a function of its physical properties.

The augmented COART model is described in Sec. 2, and its performance is contrasted against ICESCAPE and SHEBA measurements in Sec. 3, including sensitivity studies with respect to light-absorbing impurities. The conclusions are presented in Sec. 4. An appendix is also provided to show relevant sensitivity tests.

2 Radiative transfer model

The radiative transfer model used in this study is developed from COART (Jin et al., 2006), a multiple scattering code for the coupled atmosphere-ocean system based on the discrete-ordinate DISORT algorithm (Stamnes et al., 1988) but modified to account for the change in refractive index across the air-water interface. The atmosphere and the ocean each can be divided into an arbitrary number of layers, in order to resolve the vertical variation of physical properties. Treatment of absorption and multiple scattering by gasses, aerosols, and clouds in the atmosphere and CDOM, phytoplankton and non-plankton particulates in the ocean is included. The atmospheric absorption database is adopted from the MODTRAN code and has different available spectral resolutions up to 0.1 cm^{-1} (Berk et al., 2008). The ice medium has now been implemented for applications to the cryosphere, with refractive index from Warren and Brandt (2008). Since reflection and refraction processes (due to the change in refractive index) across the air-ice-water

https://doi.org/10.5194/tc-2022-106
Preprint. Discussion started: 20 June 2022

interfaces are rigorously taken into account when solving the radiative transfer equation, radiative processes in the coupled atmosphere-sea ice-ocean system are described consistently and efficiently. The ocean and ice layers are treated in the same way as the atmospheric layers, but with significantly different optical properties. The same Gaussian normal distribution used to model the ocean surface roughness (Cox and Munk, 1954) is also used to describe the slope distribution of the facets forming the ice surface. The surface roughness reduces the surface albedo because of shadowing, but this effect is non-negligible only for grazing directions of the incident light. The possible occurrence of melt ponds on top of the ice is also considered, in the form of a pure freshwater layer of any desired depth. Water absorption data is from the compilation of Pope and Fry (1997) and Smith and Baker (1981). Since COART has previously been validated for radiation studies in the atmosphere and ocean (Jin et al., 2002; 2005), in this study we focus on evaluating the performance of the newly implemented model in simulating the radiation field reflected and transmitted by the sea ice medium.

Absorption by pure ice, and scattering and absorption by brine pockets and air bubbles enclosed in the ice are at the base of the treatment. The presence of other possible inclusions (BC and phytoplankton) is also considered. The ice absorption coefficient is based on the compilation of Warren and Brandt (2008). Based on the phase equilibrium constraints, the total brine and air volumes are determined by the ice temperature, salinity and density (Cox and Weeks, 1983). The inherent optical properties (IOPs) of bubbles are obtained with Mie calculations, using a power-law size distribution (Light et al., 2003, Grenfell, 1983). Following Light et al. (2003), the bubble number distribution, $N(r_{bub})$, is represented as a function of bubble equivalent radius (r_{bub}) as:

$$N(r_{bub}) = N_0\, r_{bub}^{-1.5} \qquad (1)$$

where N_0 is determined by total air volume calculated through the Eq. (14) of Cox and Weeks (1983), that is:

$$V_{air} = \int_{r_{min}}^{r_{max}} N(r_{bub})\, r_{bub}^3\, dr_{bub} \qquad (2)$$

The minimum and maximum bubble radii are set to 0.01 mm and 1.0 mm, respectively, approximately the range observed (Light et al., 2003, Grenfell 1983). The horizontal cross-sectional area of brine inclusions can also be fitted by a power-law distribution (Light et al., 2003; Perovich and Gow, 1996). Using the effective radius of equivalent spheres (r_{bri}) with the same area distribution as in Light et al. (2003), the size distribution of brine pockets is given by the following power law:

$$N(r_{bri}) = N_0\, r_{bri}^{-2.73} \qquad (3)$$

As for the air bubbles (Eq. 2), the total brine number is determined by the total brine volume calculated from Eqs. 4 and 5 in Cox and Weeks (1983) but with the size distribution defined by the Eq. 3. Due to the large size parameter and the similar refractive indices of brine and ice in the shortwave part of the spectrum, most of the scattered light by the brine is concentrated in a very small cone around the forward direction. This forward scattering peak can be considered as "non-scattered" and added back to the incident radiation in the radiative transfer algorithm. Therefore, the actual scattering coefficient can be scaled down dramatically, which actually reduces the scattering efficiency of the brine pockets. The equivalent-sphere assumption may become problematic when brine size becomes large, but the forward scattering also becomes stronger as the size of the brine pockets increases. These factors make the error resulting from the uncertainties in brine size distribution and brine pocket shape much smaller than might be expected. As sea ice cools, solid salts may precipitate and be expelled from the brine pockets. However, the solid salt contribution only becomes significant at ice temperatures below the crystallization temperature of $NaCl.2H_zO$ (-22.9^{O}C). There is no size distribution reported for the salt; however, the cases studied here pertain to sea ice surveyed in the warm, summer season, so solid salt scattering can be neglected.

Using the size distributions (Eqs. 1 and 3), we generated look-up tables with the IOPs of brine pockets and air bubbles over the 0.25-4.0 μm spectral region. The sea ice IOPs are therefore directly associated with the ice physical properties,

https://doi.org/10.5194/tc-2022-106
Preprint. Discussion started: 20 June 2022

i.e., the temperature, salinity, and density, in turn used as the input parameters for the COART model. This physically-based approach provides a sophisticated and complete treatment to study radiative transfer in sea ice.

3 Validation studies

If both the reflection and transmission of ice are correctly modeled, the total ice absorption is correctly quantified. The spectral albedo and transmittance of sea ice are mostly influenced by its physical structure and by the angular distribution of the incident light, whereas the effects of atmospheric and oceanic particulates are less significant (except of course for very thin, optically-finite ice). For this reason, the spectral albedo and transmittance are AOPs frequently used in validation studies for understanding the radiative transfer in sea ice. We use the standard subarctic atmospheric profile as a background atmosphere, and open-ocean water properties for the ocean layers beneath the ice. The Chl-a concentration in seawater is set to 0.1 mg/m^3, about the average reported for the arctic ocean (Gordon and Morel, 1983; Morel and Maritorena, 2001; Morel and Gentili, 2004). We strived to use all available observational data to determine the input to the model, focusing on two common ice types: bare and ponded ice.

3.1 Bare ice

3.1.1 First-year ice

The gray areas in Fig. 1 show the total range of a series of albedo and transmittance measurements collected at each of two ICESCAPE stations in the Beaufort Sea: the top panels are for the 3 July 2010, and the bottom panels for the 19 July 2011 case. A melting state and the presence of ponds were reported for both these FYI surfaces along the "albedo line" connecting the collection sites, which extends to a length of 200 m. From the series of measurements, we selected those classified as bare-ice. One observation on 3 July 2010, was excluded since its very low average albedo in the visible (0.67) suggested the presence of an undetected thin water layer. The Solar Zenith Angle (SZA) is calculated based on the reported observational time and location latitude and longitude. Another available information regards the illumination conditions, which were recorded as brilliantly clear on 19 July 2011 (SZA = 53°), and completely overcast (but with visible Sun, SZA = 48°) on 3 July 2010. As shown in the Appendix, overcast conditions significantly affect the albedo only for very low or very high SZAs. The former never occur at extreme latitudes, and the SZA on 3 July 2010 (48°) is within the 45°-60° range that allows to neglect the presence of clouds in the simulations.

The strong spectral dependence of the absorption coefficients for brine, ice, water and organic or other inclusions (Grenfell and Mayakut, 1977; Perovich and Gow, 1996) is responsible for the nearly constant albedo in the visible region and the significant decrease in the near infrared region. Timco and Frederking (1995) reported FYI densities ranging from 0.84 to 0.91 g/cm^3 for the ice above the waterline, and 0.90 to 0.94 g/cm^3 for the ice below the waterline. Density was only measured on the uppermost 80 cm of the ice core during ICESCAPE and it varied between 0.625 and 0.909 g/cm^3 for FYI. To model the vertical structure of bare, melting sea ice, L08 and L15 utilize three layers corresponding to a granular, low-density surface scattering layer (SSL), a denser drained layer (DL), and a high density interior layer (IL). L08 identified the SSL, typically 1-5 cm thick, as having the largest scattering coefficient (up to two orders of magnitude larger than that of the IL). The DL roughly occupies the remainder of ice sitting above the freeboard, and the IL the rest of the column beneath the DL. The scattering coefficient values for the DL are intermediate between the SSL and IL. In order to determine the ice absorption, L08 set the ice density at 0.42, 0.83, and 0.92 g/cm^3 for the SSL, DL, and IL, respectively. The results of these simulations indicate that the (highly-scattering) SSL is critical for the radiative transfer simulation. In these studies, the refractive index is assumed to change at the SSL–DL interface. Effectively, the SSL is treated as a snow-like, granular ice layer, which has very different physical and optical properties from the rest of the ice column. The augmented COART model can rigorously account for snow on top of the ice, and therefore we can provide results that quantify the goodness of such assumption. We first consider the SSL as the same medium (ice) as the rest of the ice column, but with significantly lower bulk density (see Fig.1). To mirror the morphology described above and the input of L08 and L15, we use a 3-layer structure for the 3 July 2010 (19 July 2011) case with densities of 0.55 (0.60) g/cm^3 for the thin SSL, 0.85 (0.83) g/cm^3 for the

https://doi.org/10.5194/tc-2022-106
Preprint. Discussion started: 20 June 2022

DL, and 0.92 g/cm^3 for the IL. The thicknesses of the individual layers are set to 1 cm for the SSL, 10 cm for the DL, while the IL occupies the rest of the total thickness, which is constrained with an average of the thicknesses locally measured: 118 cm (from the individual measurements of 103 cm, 115 cm, 135 cm) on 3 July 2010, and 152 cm (149 cm, 149 cm, 157 cm) on 19 July 2011. For the salinity, we use the profiles reported from the core analysis of Polashenski et al. (2015), averaging the available data points in each model layer. Since measurements are not reported for the SSL (which normally gets destroyed when collecting the core) and the bottom of the ice, we assume the shallowest and deepest value extend to these remaining portions. Polashenski et al. (2015) also report that the core temperatures were always between 0°C and -1°C. Our tests show negligible sensitivity of the AOPs to small variations in temperature. To facilitate the comparison among all simulations, and to be consistent with the expected temperature at the ice-ocean interface, we chose a uniform temperature profile throughout the ice of -2°C.

To highlight the importance of using at least three layers, we include the results for single- and double-layered ice, with densities taken as the combinations of those used in the 3-layer model. It is clear that a single layer is insufficient to adequately reproduce both the albedo and transmittance. The 2-layer model with a low-density SSL yields a lower albedo in the visible region. Since air bubbles scatter more effectively than the brine pockets, and the air volume is closely related to the bulk ice density, the sea ice AOPs are more sensitive to the density than to the salinity or the temperature. The black curve shows the drastic improvement obtained using the 3-layer ice model described above.. Further tuning is generally possible if the number of layers is increased, although in this particular case attempts to use four layers did not appreciably improve the fit (not shown).

While L08 and L15 directly adjusted the scattering coefficient values with fixed densities in ice layers to match the observational albedo, we adjusted the ice density. Because in our approach the ice IOPs are linked to the ice properties, adjusting density would essentially change all the IOPs, including the scattering coefficient and asymmetry factor which is also fixed at 0.94 in L15. Figure 2 shows the impact of density variation in different layers on the albedo and transmittance. The gray areas correspond again to the range of the albedo and transmittance measurements acquired on 3 July 2010 (top row in Fig. 1), whereas the solid lines correspond to model results with different density profiles. Starting from the same optimal profile found in Fig. 1, here represented in black, a moderate increase in SSL density (red) reduces the albedo, with noticeable effects in the 1.0-1.4 µm region. The corresponding increase in transmittance is negligible. Changes in DL density (green) are most evident at wavelengths <1.0 µm, whereas changes in the IL density (blue) impact the visible part of the spectrum only. Although it remains challenging to simultaneously fit albedo and transmittance in an optimal way in the absence of completely measured density profiles, these results demonstrate how the augmented COART model enables a fine tuning of the AOPs.

To evaluate the assumptions made in L15, in Fig. 3 we substitute the ice SSL with a snow layer of equal density (0.6 g/cm^3). The snow is composed of spherical grains, whose size determines the albedo at absorbing wavelengths (Warren 2019). We considered grain size equal to 300 µm to represent new snow, and 1000 µm to represent aged, melting snow. Old snow yields a fairly good agreement in both albedo and transmittance (black). Increasing the snow depth to 2 cm (red) and adjusting the DL ice density (0.89 g/cm^3) improves the agreement in albedo but it increases the transmittance and has no discernible effect at longer wavelengths (>1.2 µm). Since the snow IOPs are assumed to be independent of the snow density, different combinations of snow thickness and density can produce the same albedo and transmittance. The albedo curves for the larger grain size are in closer agreement with the observations at wavelengths <1.2 µm, but consistently lower at longer wavelengths. By refining the ice and snow density profiles (i.e., increasing the number of layers), the model-observation agreement at shorter wavelengths (<1.2 µm) could be further improved. However, the albedo at longer wavelengths is determined by the thin layer of snow and the grain size is the dominant factor in this spectral region. The grain size must be reduced to <300 µm (green) in order to fit the albedo at the longest wavelengths, but the observations at middle wavelengths are then drastically overestimated. Moreover, such small grain sizes are typically associated with pristine snow, not suitable to simulate the "granular" nature of the SSL. These simulations show that the 3-layer ice model offers superior performance compared to considering a SSL composed of snow.

The simulations of sea ice albedo and transmittance shown in the previous figures tend to be higher than the observations in the visible spectrum, which indicates an underestimation of ice absorption. Black Carbon (BC) is the main component of soot-like, absorbing impurities often found deposited on snow and ice. Clarke and Noone (1985)

https://doi.org/10.5194/tc-2022-106
Preprint. Discussion started: 20 June 2022

reported soot amounts mostly in the 5–50 nanograms of carbon per gram of snow (ng g^{-1}) range, corresponding to 0.005-0.05 ppm. Doherty et al. (2010) measured BC concentrations around the Arctic (mostly in the top 50 cm of snow) ranging anywhere from 0.003 to 0.02 ppm, or occasionally even higher, from lower values near the North Pole to higher values at lower latitudes in the Arctic Ocean. The SHEBA observations show a lower average background BC of 0.0044 ppm for April snow (Grenfell et al., 2002). Desired concentrations of BC can be included in any layer of the augmented COART model, with the IOPs given in the Optical Properties of Aerosols and Clouds (OPAC) software package (Hess et al., 1998). The reduction in albedo caused by BC is a widely known effect (Warren and Wiscombe, 1980; Hansen and Nazarenko 2003). Figure 4 contains the sensitivity of albedo and transmittance caused by increasing BC mass mixing ratios (0, 0.02 ppm, 0.04 ppm). These values were calculated to span the range of average BC concentrations indicated above, uniformly redistributed in the top 10 cm of ice in the model. As expected, contamination from absorbing impurities such as soot (red and green curves) reduces the sea ice albedo and transmittance in the visible part of the spectrum, leading to an improvement in the model-observation comparison.

3.1.2 Multi-year ice

In the model, the difference between FYI and MYI is reflected in the values chosen for the total ice thickness (generally higher for MYI), the salinity and the IL density (both generally lower). Figure 5 shows a fitting attempt for two MYI cases. The black lines are albedo and transmittance measurements collected during SHEBA with two different spectroradiometers: a Spectron Engineering SE-590 (dashed) and Analytical Spectral Devices Ice-1 (solid). Typically, MYI has more cavities, due to the flushing of melt water, and is thicker than FYI; therefore, it has higher albedo and lower transmittance. A very limited number of cores were acquired during SHEBA (D. Perovich, *personal comm.*), which were not strictly co-located with the optical measurements. The salinity profiles (1 ppt and 3 ppt) were assumed in the simulations, covering the mean salinity values reported for MYI, at least in the bulk of the ice, (Eicken et al., 1995).

In the top panel of Fig. 5, the total ice thickness is 218 cm (measured in situ on 21 July, 1998). A few centimeters of surface granular layer was reported, yet no density measurements were available. As an approximation, we set the SSL thickness to 2 cm and its density to 0.6 g/cm^3. As for the FYI case, a single layer is insufficient to obtain a good agreement. For this particular case, a fairly good agreement is obtained for both the albedo and the transmittance using just two layers. A density of 0.915 g/cm^3 and salinity equal to 3 ppt is used for the lower ice layer (red). It should be noted that the transmittance through the MYI is very small (all transmittance curves are multiplied by a factor of ten), implying that its measurement uncertainty is large. Salinity in MYI can be very low because of meltwater flushing (Untersteiner, 1968) and thus we also tested the results with salinity of 1.0 ppt. For this low salinity, a slight adjustment in the lower layer density (0.910 g/cm^3) yields essentially the same agreement, indicating that the AOPs are less sensitive to the salinity than to the density (blue).

As done for the FYI case, we also tested the substitution of the SSL with a layer of snow (middle panel). Similar model-observation agreement as using ice SSL is obtained for wavelengths <1.2 μm with a large grain size (1000 μm). As noted for the curves in Fig. 3, also in this case the grain size has to be reduced to at least 300 μm to fit the measured albedo at wavelengths >1.4 μm.

In the MYI case observed on 31 July, 1998 (lower panel), the total ice thickness is 197 cm and "a few mm of new snow on surface" was reported. In our modeling, 5 mm of snow with grain size of 200 μm were considered. The ice is divided into three layers, with a 2 cm-thick (15-cm-thick) SSL (DL). The densities for the three layers are 0.80, 0.92, and 0.916 g/cm^3, respectively, and the salinity is 3 ppt. If the salinity is lowered to 1.0 ppt, a slight reduction (0.005 g/cm^3) in the middle and lower layer density produces nearly identical albedo and slightly lower transmittance. Compared with the physically thicker MYI in the upper panel, the albedo in the near infrared here is considerably higher due to the existence of few millimeters of new snow. The results show that the model correctly captures this aspect.

The systematic overestimation of the observations in the visible region indicates insufficient in-ice absorption accounted for by the model. Other species can differentially affect the spectral radiation transport within the ice column. Several observations have shown the existence of ice algae or chlorophyll pigments (Ardyna et al., 2020;

https://doi.org/10.5194/tc-2022-106
Preprint. Discussion started: 20 June 2022

Massicotte et al., 2020; Assmy et al., 2017). Large seasonal variations of algal pigments (from 0.01 mg/m^3 in April to 0.5 mg/m^3 in June) were reported, with higher concentration at the bottom and top ice layers (Perovich et al., 1998). For the MYI case shown in the upper panel of Fig. 5, Fig. 6 shows that the simple assumption of a Chl-a concentration of 0.3 mg/m^3 uniformly distributed across the ice column would significantly lower the transmittance in the visible (green lines), therefore improving the model agreement. Nevertheless, the effect on albedo is much smaller and that in the near infrared is negligible. As done for the FYI, we also tested the inclusion of BC particles in the SSL and DL (upper 18 cm, about the ice freeboard depth) with a concentration of 0.01 ppm. Both the albedo and the transmittance in the visible spectrum are reduced and the model-observation agreement is improved.

3.2 Ponded ice

The springtime increase in ambient temperature can trigger the formation of water ponds on top of the sea ice surface. Compared to white, bare ice, the albedo of ponded ice can be reduced dramatically across all shortwave wavelengths. Melt ponds occur when solar irradiance is largest, and water has much lower reflection and higher transmission than ice, impacting the solar energy distribution in the atmosphere-sea ice-ocean system. A series of observations, complete with measurements of pond depth and floor thickness, are available from ICESCAPE. The conditions ranged from completely overcast and a barely visible solar disk to a visible solar disk and clear skies.

It is reasonable to expect that the accumulation of water on top of ice should annihilate the SSL. Indeed, percolation theory predicts the ice permeability to undergo a drastic transition when the brine volume exceeds ~5% (Golden, 2001), triggering the flushing of brine pockets through an increase in pore connectivity. Nevertheless, a thin top layer of so-called “superimposed” or “interposed” ice can still be possible in the presence of refrozen snowmelt. Such processes temporarily “seal” the ice surface, with appearance effects visible even to the unaided eye (Polashenski et al., 2015), and lead to top layer thicknesses of up to 10 cm. In absence of complete observational characterization of the vertical structure, and given the interplay of density and thickness, this physical thickness was chosen to model the top layer of the cases presented here.

The rows in Fig. 7 correspond to four ICESCAPE observations (black) of ponds with different depths (melt pond depth and ice thickness are from the observational data). The total ice thickness (pond depth) for the four presented cases are 112 (8), 94 (11), 70 (20), and 70 (30) cm (top to bottom panels). The two observations for the same 20 cm pond depth on 3 July 2010 show slight difference in transmittance. The temperature at the water-ice interface at the bottom of the pond is set to 0^{o}C, and that at the bottom of the ice to -2^{o}C with a linear change through the ice column. The salinity is also from observational data, and varies from about 0.5 ppt to 3.0 ppt (Polashenski et al., 2015). The pond water is assumed to be pure freshwater with optical properties based on Pope and Fry (1997) and Smith and Baker (1981). Based on the reported overcast conditions for 2 July and 3 July (but with visible sun), a stratus cloud layer is modeled between altitudes of 0.5 km and 1.0 km with optical depth of 1.0. We found that two layers (with a top layer thickness of 10 cm) are generally sufficient. The ice density of the bottom layer is set at 0.92 g/cm^3 and the top layer density is adjusted for each case. For the thick ice with shallow pond (top row) observed on 19 July, a 3-layer ice model is required for satisfactory model-observation agreement. We use 10 cm (0.83), 70 cm (0.921 g/cm^3), and 42 cm (0.924 g/cm^3) for the top, middle and bottom layer depth (density), respectively.

It should be noted that albedo and transmittance were not measured exactly at the same location. Since the ice core thickness was reported for the transmittance measurements only, the safest assumption was to use the same thickness for the albedo simulations. This assumption limits the quality of the fit to the albedo, given the relatively thin nature of the ponded ice cases analyzed here. However, the results show that using a simple 2-layer ice model (3-layer for thick ice) the transmittance can be matched across all spectra, and the albedo agreement is satisfactory.. The albedo between 0.8 and 1.4 μm, where the observations are systematically higher than the model, is dominated by the pond water properties and is not related to small uncertainties in the measurements of ice thickness. If the albedo measurements in the near infrared are accurate, this fact indicates that some particle scattering might exist in the pond water, which is missing in the modeling. However, the large model-observation discrepancy in albedo in the visible spectrum on 3 July, 2010, might arise from inaccurate observational constraints on ice thickness and physical properties. Both the model and observation in Fig. 7 show that not only the water pond reduces the sea ice albedo, but

https://doi.org/10.5194/tc-2022-106
Preprint. Discussion started: 20 June 2022

also significantly impacts light transmission. The transmittance decreases with increasing pond depth, even if the ice thickness decreases.

4 Conclusions

This study presents the extension of a fully-coupled RT model (COART) to include a physically-based description of radiative processes within sea ice. The scattering properties of brine pockets and air bubbles, including the respective single scattering albedo and phase function, are calculated based on observed size distributions. The gas and brine volume are derived from the phase equations (Cox and Weeks, 1983) as a function of density, salinity and temperature. Therefore, the IOPs of sea ice are parameterized directly as a function of its physical properties. Light-absorbing impurities, such as BC and Chl-a, can also be included in any layer of the ice or in the snow above it. This type of contamination can be immediately extended in the model to any other inorganic particulate or taxonomic species, provided the relative tabulated absorption spectrum is available. To demonstrate the robustness of this model and its accuracy in estimating the total absorption in the ice column, its performance is evaluated against albedo and transmittance observations of FYI, MYI, and ponded ice for the visible and near-infrared range of wavelengths.

The model is highly sensitive to vertical variations in ice density, and it is found that a minimum of three layers is required to adequately simulate the albedo and transmittance for bare FYI, in agreement with previous findings. This 3-layer structure can be morphologically associated with a granular, low-density surface scattering layer (SSL), a denser drained layer (DL), and a high-density interior layer (IL). The SSL is required to model the observed albedo of bare ice in the near infrared. While previous studies used the extinction properties of a snow layer to represent the SSL (L15), we use a low-density ice layer as the topmost layer of the ice medium. Compared to the snow approach, this approach produces a higher albedo in the near infrared and thus better overall spectral agreement with the observations. To fit the albedo at the longest wavelengths (>1.4 μm), we show that the snow approach requires, at least for the examined cases, small grain sizes (≤300 μm) typical of new snow rather than of a granular layer. For MYI, an IL with lower density than for FYI is required to obtain satisfactory agreement for both albedo and transmittance. Sensitivity tests show that lower salinity values, normally associated with MYI, affect the AOPs to a much smaller extent than density does. For ponded ice, a 2-layer ice model agrees closely with the measured AOPs for a range of pond depths, with relatively thin ice (<100 cm) beneath the water. For thick ponded ice (>100 cm), a 3-layer ice model is still required for satisfactory simulations. Depending on the pond depth, the albedo (transmittance) is significantly lower (higher) than that of bare ice, and transmittance increases with pond depth for similar ice thicknesses below. The albedo is determined by the optical properties of the pond in the near infrared, and by those of the ice below in the visible. Discrepancies between model and observations in the middle wavelength range (0.8–1.4 μm) suggests the existence of particle scattering in the pond water, which is not included in the model (assuming the albedo measurements were accurate). For all ice types, when clean ice and pure water are assumed, there appears to be insufficient absorption in the visible part of the spectrum. In this respect, contamination by either BC or Chl-a very effectively reduces both the albedo and the transmittance in the visible, providing an additional degree of freedom during fitting procedures to improve the agreement with the observations.

The fine-tuning of the AOPs of sea ice as a function of the descriptive physical parameters makes the augmented COART model a valuable tool to represent the complex radiative processes in the cryosphere. From a retrieval point of view, this forward code can be embedded within an inversion scheme to provide an optimal search for the chosen set of free parameters. An accurate and efficient radiative transfer model is also required for climate models, which use simple AOP parametrizations for sea ice. The integration of a suitable form of this engine into the state-of-the-art NASA GISS ModelE (Schmidt et., 2006) is ongoing, in order to provide accurate estimates of the fluxes reflected back to the atmosphere and transmitted into the ocean, as well as the radiative absorption within the ice medium that determines the evolution of its thickness. Light et al. (2003) and L15 demonstrated that this objective could be achieved with a 3-layer ice (2-layers for ponded ice) model by directly adjusting the ice IOPs (i.e., the scattering coefficient in each layer with a fixed scattering asymmetry factor of 0.94 and a fixed density profile). Within our

https://doi.org/10.5194/tc-2022-106
Preprint. Discussion started: 20 June 2022

approach, the density is used as a tunable parameter since in situ measurements are not always available. Moreover, density is not a variable simulated by climate models, while temperature and salinity are dynamically computed. Due to the complex inter-relationships among ice physical properties, IOPs and AOPs, if the IOP parameterization is physically incorrect it is unlikely to produce simultaneous fits to albedo, transmittance, and absorption across all wavelengths. Should accurate density profiles be available, the relationships between the IOPs and the ice properties can be refined by improving, for example, the parameterizations with respect to the size distribution of air bubbles and brine inclusions. Through this process, a more robust IOP dependence on the ice physical properties can be obtained. For these reasons, this and related works advocate the deployment of comprehensive measurement suites capable of adequate data quality, especially regarding the vertical profiles of density, temperature, and salinity which are notoriously challenging. A better characterization of impurities, such as soot-like, dust-like and algal particulates is also desirable, since these contaminants are often present in the ice column as well as in melt pond waters. Fortunately, a fair share of recent campaigns have targeted this aspect, significantly augmenting available datasets for further improvements in the parameterization of the ice IOPs.

5 Data Availability

The data from the ICESCAPE campaign were obtained from the SeaWiFS Bio-optical Archive and Storage System (SeaBASS) portal (https://seabass.gsfc.nasa.gov/). The data from the SHEBA campaign were downloaded from the dedicated UCAR portal. More specifically, spectral albedo measurements were sourced at Grenfell, T., & Light, B. (2007). Spectral Albedo. Version 1.0 (Version 1.0). UCAR/NCAR - Earth Observing Laboratory. https://doi.org/10.5065/D6765CQ1; transmittance data were sourced at Perovich, D. 2007. Spectral Light Transmittance. Version 1.0. UCAR/NCAR-Earth Observing Laboratory. https://doi.org/10.5065/D6T1521W.

6 Authors' contributions

ZJ developed the COART model. ZJ and MS carried out the main bulk of the simulations. ZJ and MO wrote the manuscript, MS contributed to editing. MO retrieved the measurements data used throughout the paper, carried out the simulations for the Appendix and compiled it.

7 Competing interests

The authors declare that they have no conflict of interest.

8 Acknowledgements

This work was carried out as part of the NASA ROSES IDS (Interdisciplinary Research in Earth Science) award 80NSSC20K1523. We are grateful to Dr. Bonnie Light for continuous assistance with the interpretation of the ICESCAPE and SHEBA datasets.

Appendix

A complete report on the sensitivity of albedo and transmittance to the variables in the augmented COART model is prohibitive for the main body of the paper. For this reason, we decided to collect in this Appendix some results that justify some of the claims made in the paper. In the figures that follow, we take as reference the 3-layer model used for the July 3, 2010, case in Fig. 1 (black curve). As specified in the paper, the density of the ice layers is set to d_{SSL}=0.60, d_{DL}=0.85, and d_{IL}=0.92 g/cm^3.
Figure A1 illustrates the small sensitivity of the albedo to SZA (increasing for increasing SZA) in the visible, but measurable differences appear as the wavelength increases. The sensitivity of the transmittance is negligible. It should

https://doi.org/10.5194/tc-2022-106
Preprint. Discussion started: 20 June 2022

be noted that the clear sky is assumed here. If atmospheric clouds and aerosols are introduced, the sensitivity will be smaller (see Fig. A3 below).

In Fig. A2 we focus on the sensitivity to temperature at the top of the ice. Again, the reference curve is the case on 3 July, 2010 (black), for which the temperature is set as uniform at -2°C throughout the ice column. The red and blue curves correspond instead to the temperatures at the top of the ice of -10°C and -20°C. The temperature at the bottom is kept at -2°C, a value that very closely approximates the temperatures commonly observed at the ice/ocean interface. The temperature in each layer is the result of linear interpolation between top and bottom temperatures. The sensitivity is minimal. While using a top temperature of -10°C would slightly improve the fit to the albedo data in the visible for the cases presented in Fig. 1, the effect on transmittance is opposite. Considering the low sensitivity and for ease of comparison with the other simulations in the paper, we have therefore adopted the uniform profile with T=-2°C which also well applies to summer conditions.

Another factor worth considering, and that deals with the illumination conditions, is the presence of cloud cover. Low-level stratus clouds are very common in the Arctic summer (Curry et al., 2000). In Fig. A3 we consider the presence of a cloud layer between 0.5 and 1km in altitude, and of variable optical depths ($\boldsymbol{\tau}$=0, 1, 10). The cloud properties are calculated for droplets of effective radius equal to 10 μm (Hu and Stamnes, 1993). While the simulated spectral transmittance does not vary much (expected for ice as thick as this case, 118 cm), the sensitivity of the albedo to the different contributions of the direct and diffuse radiances to cloud optical depth is less than trivial. When a cloud is present ($\boldsymbol{\tau}$>0), the sensitivity to the SZA is reduced. Appreciable differences are noted either for very low or very high solar zenith angles, while for ~40°<SZA<~60° the albedo is essentially unaffected. The explanation of this fact resides in the Fresnel nature of the surface reflectivity. While the reflectivity for the diffuse component is insensitive to SZA and cloud optical depth, the specular reflectivity for the direct beam is rather low (and constant) for small angles of incidence (in this case, the SZA). It then decreases further around the Brewster angle, before exhibiting an almost exponential increase at grazing incidences, up to the 100% ideal limit of horizontal illumination. For increasing cloud optical depths, this non-monotonic dependence of the Fresnel reflectance on the SZA causes the albedo to increase if SZA<~40°, remain unaltered in the Brewster region (~40°<SZA<~60°), and decrease if SZA>~60°. For the observation on 3 July, 2010, the SZA was 48°, eliminating the need to consider a cloud layer in the model.

References

Ardyna, M., Mundy, C. J., Mayot, N., Matthes, L. C., Oziel, L., Horvat, C., Leu, E., Assmy, P., Hill, V., Matrai, P., Gale, M., Melnikov, I., & Arrigo, K. (2020). Under-ice phytoplankton blooms: Shedding light on the "invisible" part of Arctic primary production. *Frontiers in Marine Science*, *7*, 1-25. https://doi.org/10.3389/fmars.2020.608032.

Arrigo, K. R., Perovich, D. K., Pickart, R. S., Brown, Z. W., van Dijken, G. L., Lowry, K. E., Mills, M. M., Palmer, M. A., Balch, W. M., Bahr, F., Bates, N. R., Benitez-Nelson, C., Bowler, B., Brownlee, E., Ehn, J. K., Frey, K. E., Garley, R., Laney, S. R., Lubelczyk, L., … Swift, J. H. (2012). Massive phytoplankton bloom under Arctic sea ice. *Science (New York, N.Y.)*, *336*(6087), 1408. https://doi.org/10.1126/science.1215065.

Assmy, P., Fernández-Méndez, M., Duarte, P., Meyer, A., Randelhoff, A., Mundy, C. J., Olsen, L. M., Kauko, H. M., Bailey, A., & Chierici, M. (2017). Leads in Arctic pack ice enable early phytoplankton blooms below snow-covered sea ice. *Scientific Reports*, *7*(1), 1-9.

Ballabrera-Poy, J., Murtugudde, R., Zhang, R.-H., & Busalacchi, A. J. (2007). Coupled ocean–atmosphere response to seasonal modulation of ocean color: impact on interannual climate simulations in the Tropical Pacific. *American Meteorological Society*, *20*(2), 353-374. https://doi.org/10.1175/JCLI3958.1.

Berk, A., Anderson, G. P., Acharya, P. K., & Shettle, E. P. (2008). *MODTRAN5 version 2 User's Manual*. Spectral Sciences, Inc., and Air Force Geophysics Laboratory Doc., 99 pp.

Briegleb, B. P., & Light, B. (2007). A Delta-Eddington Multiple Scattering Parameterization for Solar Radiation in the Sea Ice Component of the Community Climate System Model. *(No. NCAR/TN-472+STR). University Corporation for Atmospheric Research*. http://doi.org/10.5065/D6B27S71.

Carnat, G., Papakyriakou, T., Geilfus, N., Brabant, F., Delille, B., Vancoppenolle, M., Gilson, G., Zhou, J., & Tison, J. (2013). Investigations on physical and textural properties of Arctic first-year sea ice in the Amundsen Gulf, Canada,

November 2007–June 2008 (IPY-CFL system study). *Journal of Glaciology*, *59*(217), 819-837. https://doi.org10.3189/2013JoG12J148.

Clarke, A. D., & Noone, K. J. (1985). Soot in the Arctic snowpack: A cause for perturbations in radiative transfer. *Atmospheric Environment*, *19*(12), 2045-2053. https://doi.org/10.1016/0004-6981(85)90113-1.

Cohen, J., Screen, J. A., Furtado, J. C., Barlow, M., Whittleston, D., Coumou, D., Francis, J., Dethloff, K., Entekhabi, D., Overland, J., & Jones, J. (2014). Recent Arctic Amplification and Extreme Mid-latitude Weather. *Nature Geoscience*, *7*, 627-637. https://doi.org/10.1038/ngeo2234.

Cox, C. S., & Munk, W. H. (1954). Measurement of the Roughness of the Sea Surface from Photographs of the Sun's Glitter. *Journal of the Optical Society of America*, *44*, 838-850.

Cox, G.F. N., & Weeks, W. F. (1974). Salinity variations in sea ice. *Journal of Glaciology*, *13*(67), 109-120.

Cox, G.F. N., & Weeks, W. F. (1983). Equations for determining the gas and brine volumes in sea-ice samples. *Journal of Glaciology*, *29*(306-316).

Curry, J. A., Hobbs, P. V., King, M. D., Randall, D. A., & Minnis, P. (2000). FIRE Arctic Clouds Experiment. *Bulletin of the American Meteorological Society*, *81*, 5-29.

Curry, J. A., Schramm, J. L., & Ebert, E. E. (1995). Sea ice-albedo climate feedback mechanism. *Journal of Climate*, *8*(2), 240-247. https://doi.org/10.1175/1520-0442(1995)008%3C0240:SIACFM%3E2.0.CO;2.

Daly, S. F. (1994). Frazil Ice Dynamics. *CRREL Spec. Rep, 94-23*, 19-24.

Déry, S. J., & Brown, R. D. (2007). Recent Northern Hemisphere snow cover extent trends and implications for the snow-albedo feedback. *Geophysical Research Letters*, *34*(L22504). https://doi.org/10.1029/2007GL031474.

Dmitrenko, I. A., Wegner, C., Kassens, H., Kirillov, S. A., Krumpen, T., Heinemann, G., Helbig, A., Schroder, D., Holemann, J., Klagge, T., Tyshko, K. P., & Busche, T. (2010). Observations of supercooling and frazil ice formation in the Laptev Sea coastal polynya. *Journal of Geophysical Research: Oceans*, *115*(C05015). http://doi.org/10.1029/2009JC005798.

Doherty, S. J., Grenfell, T. C., Forsström, S., Hegg, D. L., Brandt, R. E., & Warren, S. G. (2013). Observed vertical redistribution of black carbon and other insoluble light-absorbing particles in melting snow. *Journal of Geophysical Research: Atmospheres*, *118*. https://doi.org/10.1002/jgrd.50235.

Doherty, S. J., Warren, S. G., Grenfell, T. C., Clarke, A. D., & Brandt, R. E. (2010). Light-absorbing impurities in Arctic snow. *Atmospheric Chemistry and Physics*, *10*, 11647-11680. https://doi.org/10.5194/acp-10-11647-2010.

Ehn, J. K., Granskog, M. A., Papakyriakou, T., Galley, R., & Barber, D. G. (2006). Surface albedo observations of Hudson Bay landfast sea ice during the spring melt. *Annals of Glaciology*, *44*, 23-29. https://doi.org/10.3189/172756406781811376.

Eicken, H., Lensu, M., Lepparanta, M., Tucker, III, W. B., Gow, A. J., & Salmela, O. (1995). Thickness, structure, and properties of level summer multiyear ice in the Eurasian sector of the Arctic Ocean. *Journal of Geophysical Research*, *100*(C11), 22,697-22,710.

Falkowski, P. G., & Raven, J. A. (1997). *Aquatic Photosynthesis*. Oxford: Blackwell.

Fetterer, F., Knowles, K., Meier, W., & Savoie, M. (2002). *Sea Ice Index*. National Snow and Ice Data Center. Boulder, Colorado. https://nsidc.org/data/g02135.

Flanner, M. G., Zender, C. S., Renderson, J. T., & Rasch, P. J. (2007). Present Day Climate Forcing and Response from Black Carbon in Snow. *Journal of Geophysical Research*, *112*(D11202). https://doi.org/10.1029/2006JD008003.

Gordon, H., & Morel, A. (1983). Remote Assessment of Ocean Color for Interpretation of Satellite Visible Imagery: A Review, Lecture Notes on Coastal and Estuarine Studies (Vol. 4). Springer New York. https://doi.org/10.1007/978-1-4684-6280-7.

Golden, K. M. (2001), Brine percolation and the transport properties of sea Ice, Ann. Glaciol.33,28–36, doi:10.3189/172756401781818329.

Grenfell, T. C. (1983). A theoretical model of the optical properties of sea ice in the visible and near infrared. *Journal of Geophysical Research*, *88*, 9723-9735.

Grenfell, T. C. (1991). A radiative transfer model for sea ice with vertical structure variations. *Journal of Geophysical Research*, *96*(C9), 16,991-17,001.

Grenfell, T. C., Light, B., & Sturm, M. (2002). Spatial distribution and radiative effects of soot in the snow and sea ice during the SHEBA experiment. *Journal of Geophysical Research*, *107*(C10), 8032. https://doi.org/10.1029/2000JC000414.

Grenfell, T. C., & Maykut, G. A. (1977). The optical properties of ice and snow in the Arctic Basin. *Journal of Glaciology*, *18*, 445-463.

Grenfell, T. C., & Perovich, D. K. (1984). Spectral albedos of sea ice and incident solar irradiance in the Southern Beaufort Sea. *Journal of Geophysical Research*, *89*(C3), 3573-3580.

Grenfell, T. C., Warren, S. G., & Mullen, P. C. (1994). Reflection of solar radiation by the Antarctic snow surface at ultraviolet, visible, and near infrared wavelengths. *Journal of Geophysical Research*, *99*, 18,669-18,684.

Hall, A. (2004). The Role of Surface Albedo Feedback in Climate. *Journal of Climate*, *17*, 1550-1568. https://doi.org/10.1175/1520-0442(2004)017%3C1550:TROSAF%3E2.0.CO;2.

Hansen, J., & Nazarenko, L. (2004). Soot climate forcing via snow and ice albedos. *Proceedings of the National Academy of Sciences*, *101*(2), 423-428. https://doi.org/10.1073/pnas.2237157100.

Hamre, B., Winther, J. G., Gerland, S., Stamnes, J. J., & Stamnes, K. (2004). Modeled and measured optical transmittance of snow-covered first-year sea ice in Kongsfjorden, Svalbard. *Journal of Geophysical Research*, *109*, C10006. http://doi.org/10.1029/2003JC001926.

Hamre, B., Stamnes, S., Stamnes, K., & Stamnes, J. (2017). AccuRT: A versatile tool for radiative transfer simulations in the coupled atmosphere-ocean system. *AIP Conference Proceedings*, *1810*, 120002. https://doi.org/10.1063/1.4975576.

Hess, M., Koepke, P., & Schult, I. (1998). Optical Properties of Aerosols and Clouds: The Software Package OPAC. *Bulletin of the American Meteorological Society*, *79*(5), 831-844.

Holland, M., & Bitz, C. M. (2003). Polar amplification of climate change in coupled models. *Climate Dynamics*, *21*, 221-232.

Hu, Y. X., & Stamnes, K. (1993). An Accurate Parameterization of the Radiative Properties of Water Clouds Suitable for Use in Climate Models, *Journal of Climate*, *6*(4), 728-742.

Hunke, E. C., Notz, D., Turnner, A. K., & Vancoppenolle, M. (2011). The multiphase physics of sea ice: a review for model developers. *The Cryosphere*, *5*, 989-1009. https://doi.org/10.5194/tc-5-989-2011.

Inoue, J., Kikuchi, T., & Perovich, D. K. (2008). Effect of heat transmission through melt ponds and ice on melting during summer in the Arctic Ocean. *Journal of Geophysical Research*, *113*(C05020). https://doi.org/10.1029/2007JC004182.

Jin, Z., Charlock, T. P., & Rutledge, K. (2002). Analysis of broadband solar radiation and albedo over the ocean surface at COVE. *Journal of Atmospheric and Oceanic Technology*, *19*, 1585-1601.

Jin, Z., Charlock, T. P., Rutledge, K., Cota, G., Kahn, R., Redemann, J., Zhang, T., Rutan, D. A., & Rose, F. (2005). Radiative Transfer Modeling for the CLAMS Experiment. *Journal of the Atmospheric Sciences*, *62*(4), 1053-1071.

Jin, Z., Charlock, T. P., Rutledge, K., Stamnes, K., & Wang, Y. (2006). An analytical solution of radiative transfer in the coupled atmosphere-ocean system with a rough surface. *Applied Optics*, *45*, 7443-7455.

Jin, Z., Stamnes, K., Weeks, W. F., & Tsay, S. C. (1994). The effects of sea ice on the solar energy budget in the atmosphere-sea ice-ocean system: A model study. *Journal of Geophysical Research*, *99*, 25,281-25,294.

Kauko, H. M., Taskjelle, T., Assmy, P., Pavlov, A. K., Mundy, C. J., Duarte, P., Fernández-Méndez, M., Olsen, L. M., Hudson, S. R., Johnsen, G., Elliot, A., Wang, F., & Granskog, M. A. (2017). Windows in Arctic sea ice: Light transmission and ice algae in a refrozen lead. *Journal of Geophysical Research: Biogeosciences*, *122*, 1486–1505. https://doi.org/10.1002/2016JG003626.

Kwok, R., & Untersteiner, N. (2011). The Thinning of Arctic Sea Ice. *Physics Today*, *64*, 36-41. http://doi.org/10.1063/1.3580491.

Light, B., Maykut, G. A., & Grenfell, T. C. (2003). Effects of temperature on the microstructure of first-year Arctic sea ice. *Journal of Geophysical Research*, *108*(C2), 3051. http://doi.org/10.1029/2001JC000887.

Light, B., Grenfell, T. C., & Perovich, D. K. (2008). Transmission and absorption of solar radiation by Arctic sea ice during the melt season. *Journal of Geophysical Research: Oceans*, *113*, C03023. https://doi.org/10.1029/2006JC003977.

Light, B., Perovich, D. K., Webster, M. A., Polashenski, C., & Dadic, R. (2015). Optical properties of melting first-year Arctic sea ice. *Journal of Geophysical Research: Oceans*, *120*, 7657-7675. http://doi.org/10.1002/2015JC011163.

Massicotte, P., Amiraux, R., Amyot, M. P., Archambault, P., Ardyna, M., Arnaud, L., Artigue, L., Aubry, C., Ayotte, P., Bécu, G., Bélanger, S., Benner, R., Bittig, H. C., Bricaud, A., Brossier, E., Bruyant, F., Chauvaud, L., Christiansen-Stowe, D., Claustre, H., … Babin, M. (2020). Green Edge ice camp campaigns: understanding the processes controlling the under-ice Arctic phytoplankton spring bloom. *Earth System Science Data*, *12*(1), 151-176. https://doi.org/10.5194/essd-12-151-2020.

Morel, A., & Gentili, B. (2004). Radiation transport within oceanic (case 1) water. *Journal of Geophysical Research*, *109*(C06008). http://doi.org/10.1029/2003JC002259.

Morel, A., & Maritorena, S. (2001). Bio-optical properties of oceanic waters: A reappraisal. *Journal of Geophysical Research*, *106*, 7163-7180. http://doi.org/10.1029/2000JC000319.

Nakamoto, S., Prasana Kumar, S., Oberhuber, J. M., Muneyama, K., & Frouin, R. (2000). Chlorophyll control of sea surface temperature in the Arabian Sea in a mixed layer isopycnal general circulation model. *Geophysical Research Letters*, *27*, 747–750. http://doi.org/10.1029/1999GL002371.

Nicolaus, M., Gerland, S., Hudson, S. R., Hanson, S., Haapala, J., & Perovich, D. K. (2010). Seasonality of spectral albedo and transmittance as observed in the Arctic Transpolar Drift in 2007. *Journal of Geophysical Research*, *115*, C11011. https://doi.org/doi:10.1029/2009JC006074.

Nicolaus, M., Katlein, C., Maslanik, J., & Hendricks, S. (2012). Changes in Arctic sea ice result in increasing light transmittance and absorption. *Geophysical Research Letters*, *39*(24), L24501. http://dx.doi.org/10.1029/2012GL053738.

Nicolaus, M., Perovich, D. K., Spreen, G., Granskog, M. A., Albedyll, L. V., Angelopoulos, M., Anhaus, P., Arndt, S., Belter, H. J., Bessonov, V., Birnbaum, G., Brauchle, J., Calmer, R., Cardellach, E., Cheng, B., Clemens-Sewall, D., Dadic, R., Damm, E., de Boer, G., … Wendisch, M. (2022). Overview of the MOSAiC expedition: Snow and sea ice. *Elementa: Science of the Anthropocene*, *10*(1). https://doi.org/10.1525/elementa.2021.000046.

Notz, D., & Worster, M. G. (2008). In situ measurements of the evolution of young sea ice. *Journal of Geophysical Research*, *113*(C03001). https://doi.org/10.1029/2007JC004333.

Pope, R. M., & Fry, E. S. (1997). Absorption spectrum (380-700 nm) of pure water. II. Integrating cavity measurements. *Applied Optics*, *36*, 8710-8723.

Perovich, D. K. (1996). Optical properties of sea ice. Tech. Rep. 96-1, U.S. Army Corps of Eng., Cold Reg. Res. Eng. Lab., Hanover, N. H.

Perovich, D. K., & Gow, A. J. (1996). A quantitative description of sea ice inclusions. *Journal of Geophysical Research*, *101*, 18,327-18,343.

Perovich, D. K., Grenfell, T. C., Light, B., & Hobbs, P. V. (2002). Seasonal evolution of the albedo of multiyear Arctic sea ice. *Journal of Geophysical Research*, *107*(C10), 8044. http://doi.org/10.1029/2000JC000438.

Perovich, D. K., Roesler, C. S., & Pegau, W. S. (1998). Variability in Arctic sea ice optical properties. *Journal of Geophysical Research*, *103*, 1193-1208.

Persson, P.O. G., Fairall, C. W., Andreas, E. L., Guest, P. S., & Perovich, D. K. (2002). Measurements near the Atmospheric Surface Flux Group tower at SHEBA: Near surface conditions and surface energy budget. *Journal of Geophysical Research*, *107*, 8045.

Pistone, K., Eisenman, I., & Ramanathan, V. (2014). Observational Determination of Albedo Decrease Caused by Vanishing Arctic Sea Ice. *Proceedings of the National Academy of Sciences of the United States of America*, *11*. http://doi.org/10.1073/pnas.1318201111.

Pithan, F., & Mauritsen, T. (2014). Arctic amplification dominated by temperature feedbacks in contemporary climate models. *Nature*, *7*, 181-184. https://doi.org/10.1038/ngeo2071.

Polashenski,, C., Perovich, D., & Courville, Z. (2012). The mechanisms of sea ice melt pond formation and evolution. *Journal of Geophysical Research*, *117*(C01001). https://doi.org/10.1029/2011JC007231.

Polashenski, C., Perovich, D. K., Frey, K., Cooper, L. W., Logvinova, C. I., Dadic, R., Light, B., Kelly, H. P., Trusel, L. D., & Webster, M. (2015). Physical and morphological properties of sea ice in the Chukchi and Beaufort Seas

https://doi.org/10.5194/tc-2022-106
Preprint. Discussion started: 20 June 2022

during the 2010 and 2011 NASA ICESCAPE missions. *Deep Sea Research Part II: Topical Studies in Oceanography*, *118*, 7-17. https://doi.org/10.1016/j.dsr2.2015.04.006

Schmidt,, G. A., Ruedy, R., Hansen, J. E., Aleinov, I., Bell, N., Bauer, M., Bauer, S., Cairns, B., Canuto, V., Cheng, Y., Del Genio, A., Faluvegi, G., Friend, A. D., Hall, T. M., Hu, Y., Kelly, M., Kiang, N. Y., Koch, D., Lacis, A. A., … Yao, M. S. (2006). Present day atmospheric simulations using GISS ModelE: Comparison to in-situ, satellite and reanalysis data. *Journal of Climate*, *19*, 153-192. https://doi.org/10.1175/JCLI3612.1.

Schmidt, S., Taylor, P., Boisvert-McPartland, L., Bucholtz, A., Cesana, G., DeMott, P., Fridland, A., Kahn, R., Kurtz, N., McFarquhar, G., Moore, R., Parker, C., Redemann, J., Segal-Rozenhaimer, M., Soloman, A., Tilling, R., Zamora, L., & Zuidema, P. (2020). Arctic Radiation-Cloud-Aerosol-Surface Interaction Experiment (ARCSIX) Concept. *White Paper for NASA Aircraft Investigation*. https://airbornescience.nasa.gov/sites/default/files/documents/ARCSIX_wp_20201030.p.

Serreze, M., & Barry, R. G. (2011). Processes and Impacts of Arctic Amplification: A Research Synthesis. *Global and Planetary Change*, *77*, 85-96. https://doi.org/10.1016/j.gloplacha.2011.03.004.

Smith, R. C., & Baker, K. S. (1981). Optical properties of the clearest natural waters (200–800 nm). *Applied Optics*, *20*(2), 177-184. https://doi.org/10.1364/AO.20.000177.

Stamnes, K., Tsay, S. C., Wiscombe, W. J., & Jayaweera, K. (1988). Numerically stable algorithm for discrete-ordinate-method radiative transfer in multiple scattering and emitting layered media. *Applied Optics*, *27*, 2502-2509.

Stroeve, J., Kattsov, V., Barrett, A., Serreze, M., Pavlova, T., Holland, M., & Meier, W. N. (2012). Trends in Arctic Sea Ice Extent from CMIP5, CMIP3 and Observations. *Geophysical Research Letters*, *39*, L16502. https://doi.org/10.1029/2012GL052676.

Timco, G. W., & Frederking, R.M. W. (1996). A review of sea ice density. *Cold Regions Science and Technology*, *24*(1), 1-6. https://doi.org/10.1016/0165-232X(95)00007-X.

Taskjelle, T., Hudson, S. R., Granskog, M. A., Nicolaus, M., Lei, R., Gerland, S., Stamnes, J. J., & Hamre, B. (2015). Spectral albedo and transmittance of thin young Arctic sea ice. *Journal of Geophysical Research: Oceans*, *121*(1), 540–553.

Tucker III, W. B., Cow, A. J., & Weeks, W. F. (1987). Physical properties of summer sea ice in the Fram Strait. *Journal of Geophysical Research*, *92*, 6787-6803. https://doi.org/10.1029/JC092iC07p06787.

Untersteiner, N. (1968). Natural desalination and equilibrium salinity profile of perennial sea ice. *Journal of Geophysical Research*, *73*, 1251– 1257.

Untersteiner, N., Thorndike, A. S., Rothrock, D. A., & Hunkins, K. L. (2007). AIDJEX Revisited: A Look Back at the U.S.-Canadian Arctic Ice Dynamics Joint Experiment 1970–78. *ARCTIC*, *60*(3), 327-336.

Warren, S. G., & Brandt, R. E. (2008). Optical constants of ice from the ultraviolet to the microwave: A revised compilation. *Journal of Geophysical Research*, *113*, D14220. https://doi.org/10.1029/2007JD009744.

Warren, S. G. (2019). Optical properties of ice and snow. *Philosophical Transactions Of The Royal Society A*, *377*, 20180161. http://dx.doi.org/10.1098/rsta.2018.0161.

Weeks, W. F., & Ackley, S. F. (1986). The growth, structure and properties of sea ice. *The geophysics of sea ice*, *146*, 9-164.

Warren, S. G., & Wiscombe, W. J. (1980). A Model for the Spectral Albedo of Snow. II: Snow Containing Atmospheric Aerosols, *Journal of Atmospheric Sciences*, *37*(12), 2734-2745.

https://doi.org/10.5194/tc-2022-106
Preprint. Discussion started: 20 June 2022

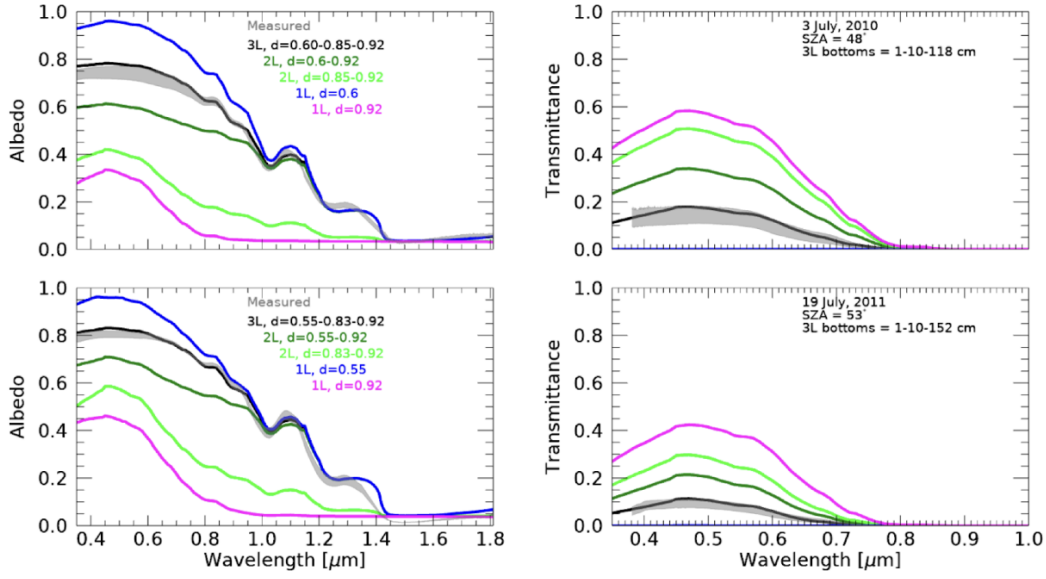

643

644 **Figure 1: Modeled spectral albedo and transmittance versus ICESCAPE FYI data (gray). The observations took place in**
645 **the Beaufort Sea on 3 July 2010 (top panels, Station 68), and 19 July 2011 (bottom panels, Station 129). An ice model**
646 **consisting of three layers (black) is needed to obtain an adequate fit. The results for 1-layer (blue and magenta) and 2-layer**
647 **(green and lime) models with different combinations of the densities used in the 3-layer model are added for comparison.**

https://doi.org/10.5194/tc-2022-106
Preprint. Discussion started: 20 June 2022

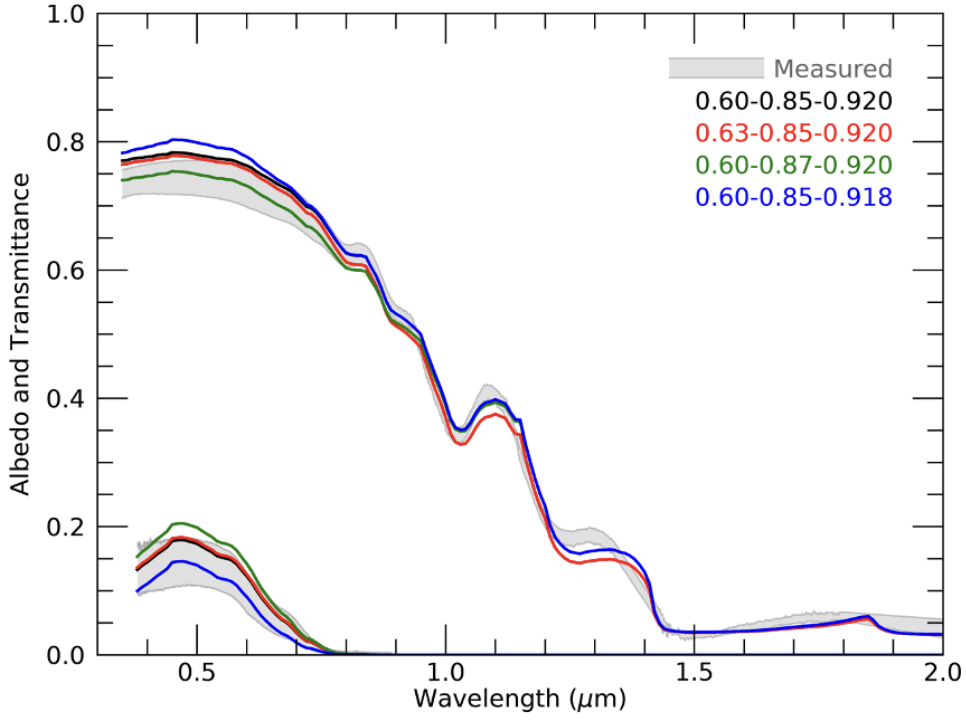

Figure 2: Effect of different ice density profiles (colored curves) on modeled albedo and transmittance. The gray areas show the maximum range of measurements collected on 3 July 2010 at a bare, FYI ice site.

https://doi.org/10.5194/tc-2022-106
Preprint. Discussion started: 20 June 2022

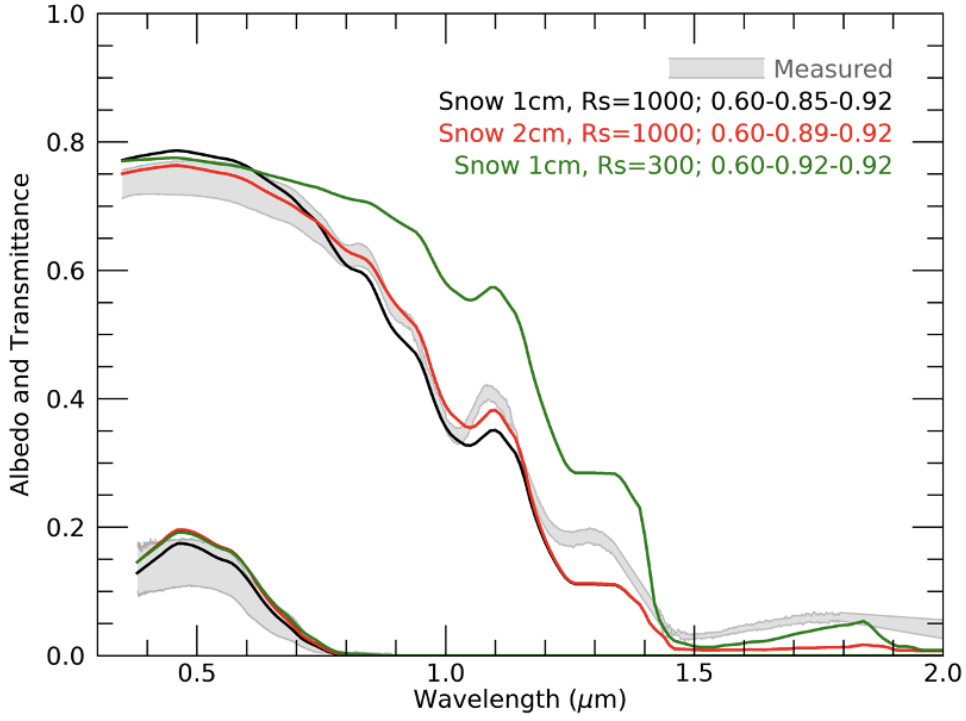

652

653 **Figure 3: As in Fig.2, but for a SSL of the indicated thickness and consisting of spherical snow grains whose density does**
654 **not vary with depth. Snow thickness and effective radius Rs (in μm) used in the model are listed.**

https://doi.org/10.5194/tc-2022-106
Preprint. Discussion started: 20 June 2022

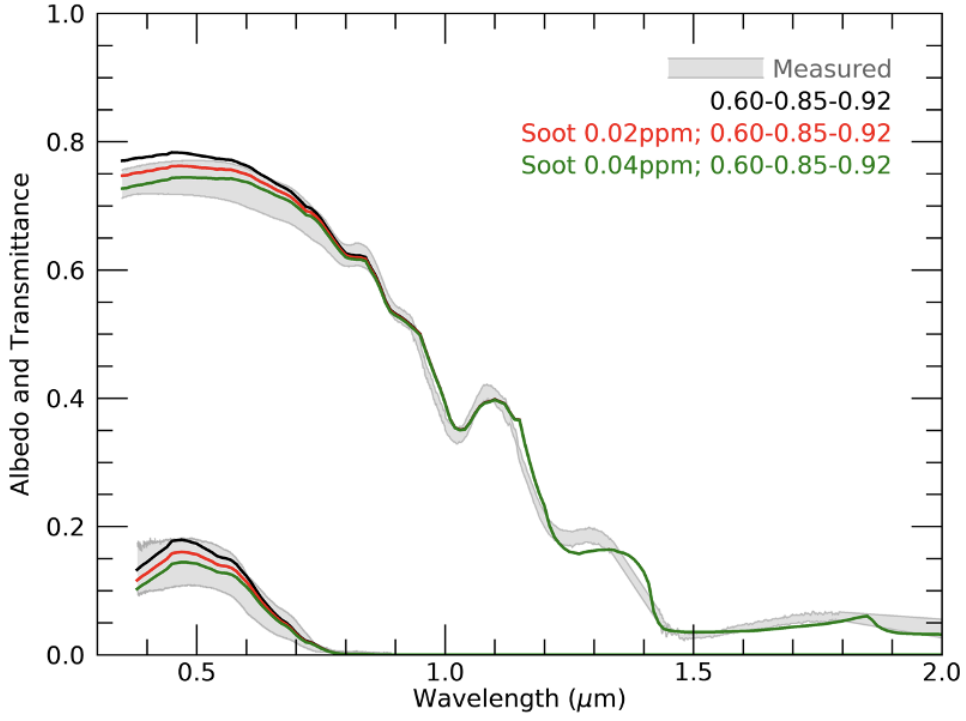

655

656 **Figure 4: As in Fig. 2, but considering added contamination from soot-like, BC particulate.**

https://doi.org/10.5194/tc-2022-106
Preprint. Discussion started: 20 June 2022

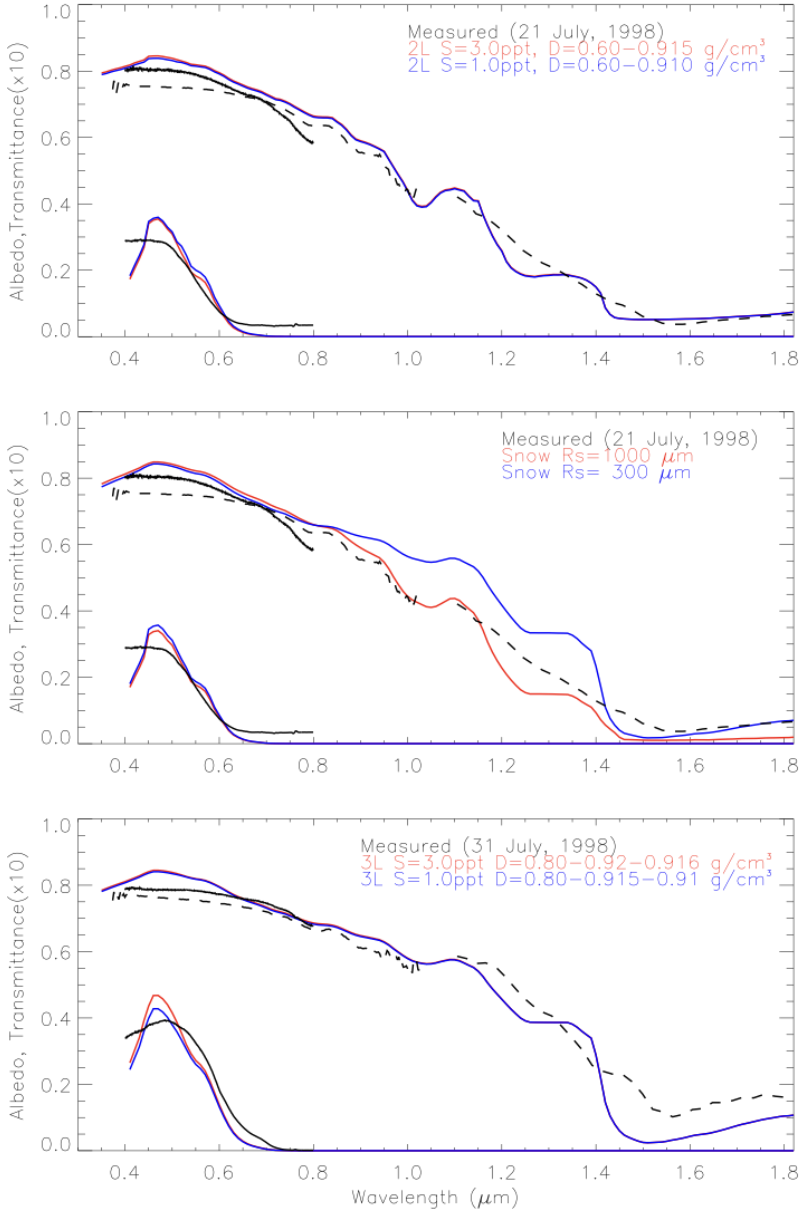

657

658 **Figure 5: Comparison of modeled (colored lines) sea ice albedo (upper lines in each panel) and transmittance (lower lines**
659 **in each panel) with SHEBA measurements of MYI (black curves). For clarity, all the transmittance curves are multiplied**
660 **by a factor of ten. *Top panel*: MYI on 21 July 1998 (thickness 2.18 m), modeled with 2 ice layers. The red and blue represent**
661 **two different salinities used in modeling. *Middle panel*: same as for the top panel, but with the ice SSL replaced by a snow**
662 **layer For grain size 300 micrometers (blue), the snow thickness is reduced to 1cm. *Bottom panel*: 3-layer results for MYI**
663 **observed on 31 July, 1998 (ice thickness 1.97 m) with 5 mm of new snow.**

https://doi.org/10.5194/tc-2022-106
Preprint. Discussion started: 20 June 2022

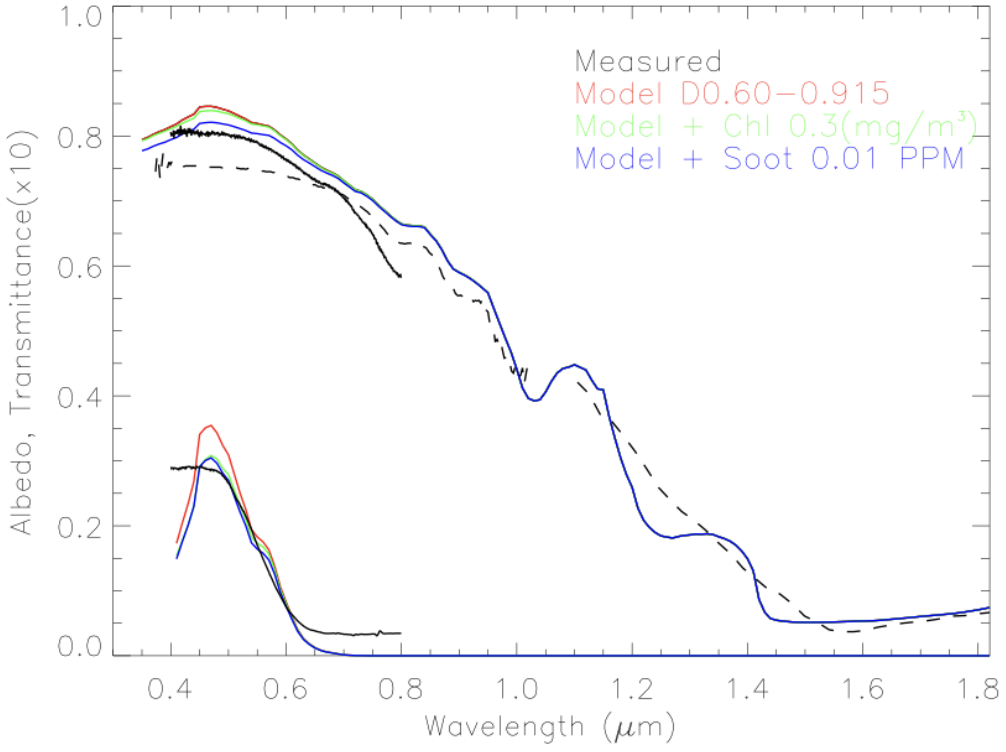

664

665 **Figure 6: Model sea ice albedo and transmittance against SHEBA measurements (black) of MYI. Red: model results with**
666 **a 2-layer ice model as shown in Fig. 5. Green: same, but with ice algae included ([Chl-a]=0.3 mg/m^3). Blue: same, but with**
667 **0.01 ppm of BC in the top 18 cm of ice. For clarity, all the transmittance curves are multiplied by a factor of 10.**

https://doi.org/10.5194/tc-2022-106
Preprint. Discussion started: 20 June 2022

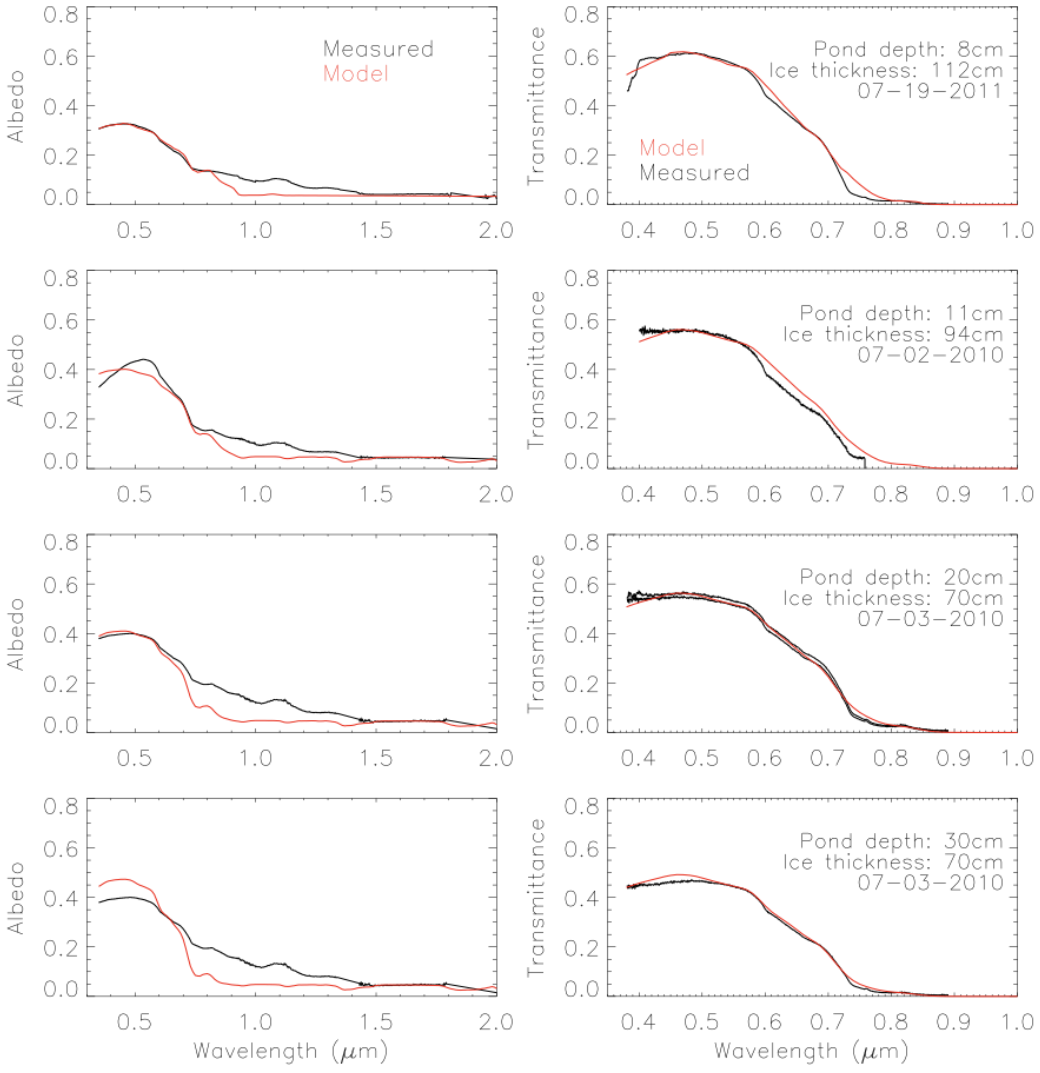

668

669 **Figure 7: Model albedo and transmittance against ICESCAPE measurements of ponded ice. The model (red) is constrained**
670 **using the measured pond depth and ice thickness, and salinity. The ice underlying the melt ponds is subdivided into only**
671 **two layers for lower three rows and three layers for the top row, all with top layer depth of 10 cm. See text for more**
672 **information.**

https://doi.org/10.5194/tc-2022-106
Preprint. Discussion started: 20 June 2022

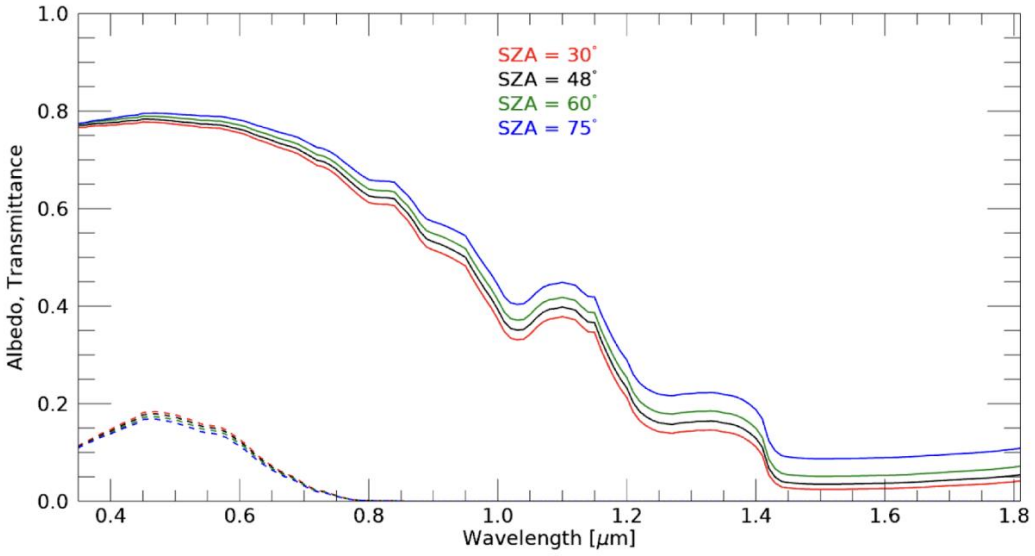

673

674 **Figure A1: Sensitivity of the model curves in Fig. 1 (black, corresponding to the July 3, 2010, case) to the Solar Zenith Angle**
675 **(SZA = 30°, 48°, 60°, 75°). Solid lines are for albedo and dashed lines are for transmittance.**

https://doi.org/10.5194/tc-2022-106
Preprint. Discussion started: 20 June 2022

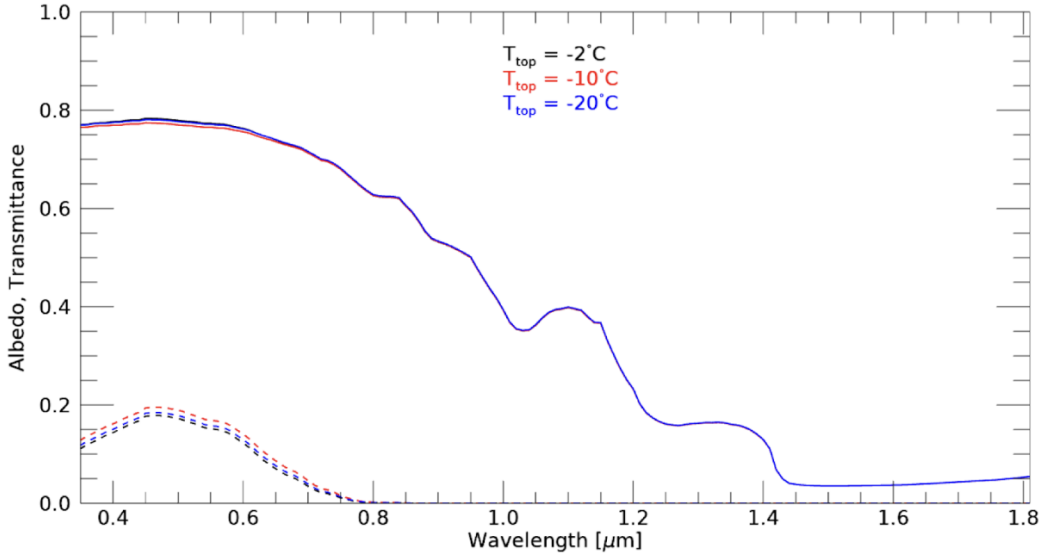

676

677 **Figure A2: As in Fig. A1, but for a SZA = 48° and temperature variations at the top of the ice (T=-2°C,-10°C, -20°C).**

https://doi.org/10.5194/tc-2022-106
Preprint. Discussion started: 20 June 2022

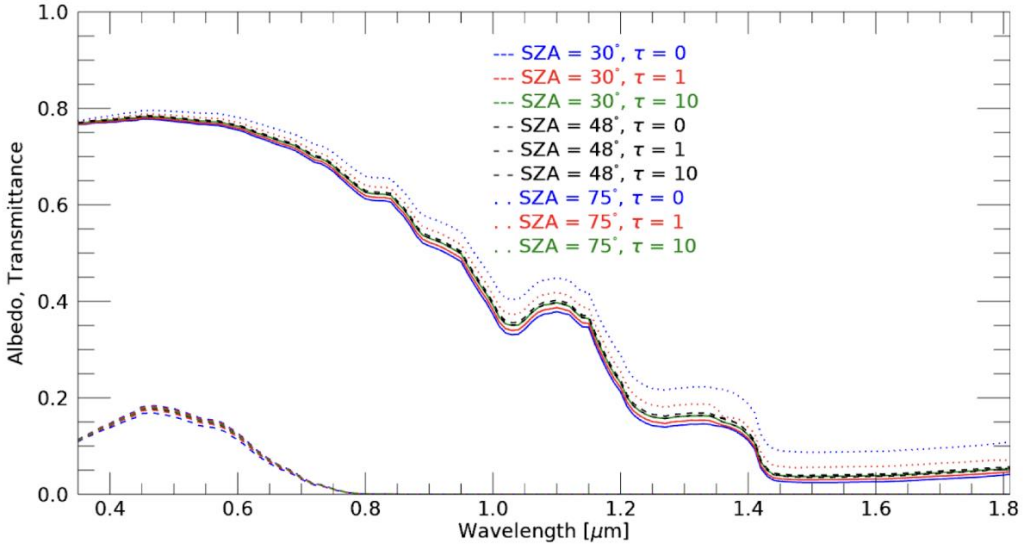

678

679 **Figure A3: Sensitivity of the albedo nd transmittance to cloud cover of variable optical depth (τ=0, 1, 10), and for different**
680 **SZAs. The three curves for SZA=48° essentially overlap and are all shown with black dashed lines. Note the opposite effect**
681 **of increasing cloud optical depth on the albedo for low and high SZAs, here set to SZA=20° (solid lines) and SZA=75°**
682 **(dotted lines).**

683